Human–robot interaction based on wearable IMU sensor and laser range finder

Carlos A. Cifuentes [a,*], Anselmo Frizera [a], Ricardo Carelli [b], Teodiano Bastos [a]

[a] *Electrical Engineering Department at the Federal University of Espírito Santo, Vitória, ES, 29075-910, Brazil*
[b] *Institute of Automatics, National University of San Juan, San Juan, 5400, Argentina*

HIGHLIGHTS

- We present a new HRI strategy based on data fusion from a wearable IMU and a LRF.
- We propose a new mobile robot controller for tracking in front of the human.
- We present an experimental validation of the fusion strategy and control system.
- We demonstrate the mobile robot controller effectiveness and stability.

ARTICLE INFO

ABSTRACT

Service robots are not only expected to navigate within the environment, as they also will may with people. Human tracking by mobile robots is essential for service robots and human interaction applications. In this work, the goal is to add a more natural robot–human following in front based on the normal human gait model. This approach proposes implementing and evaluating a human–robot interaction strategy, using the integration of a LRF (Laser Range Finder) tracking of human legs with wearable IMU (Inertial Measurement Unit) sensors for capturing the human movement during the gait. The work was carried out in four stages: first, the definition of the model of human–robot interaction and the control proposal were developed. Second, the parameters based on the human gait were estimated. Third, the robot and sensor integration setup are also proposed. Finally, the description of the algorithm for parameters detection is presented. In the experimental study, despite of the continuous oscillation during the walking, the parameters estimation was precise and unbiased, showing also repeatability with human linear velocities changes. The controller was evaluated with an eight-shaped curve, showing the stability of the controller even with sharp changes in the human path during real experiments.

1. Introduction

In 2011, about 2.5 million of service robots for personal and domestic use were sold. This represents an increase of 15% when comparing to 2010 [1]. Accordingly, the use of robots is extending from the industrial field to living and working places. In this context, intelligent service robotics is a research field that became very popular over the past years, and covers a wide range of scenarios such as: interactive guiding robots in museums [2], exhibitions [3] and shopping malls [4].

In the same manner, several research projects in many countries are focused on robots to assist elderly and/or people with disabilities. Sales on this important future market of service robots are expected to reach 4600 units in the period of 2013–2015 as this market is expected to grow substantially within the next 20 years [1]. In this scenario, mobile robots are expected to cover a wide range of applications, such as hospital support [5] and assistance for elderly people [6].

Regarding the sensor system for these applications, the development of wearable IMU (Inertial Measurement Unit) systems presents important advantages in the field of human motion analysis such as: portability, high accuracy and ease of use in unstructured environments. The integration of wearable sensors and

* Corresponding author. Tel.: +55 2733352072.
E-mail addresses: cacifuentes@gmail.com, carlos.garcia@ufes.br
(C.A. Cifuentes), anselmo@ele.ufes.br (A. Frizera), rcarelli@inaut.unsj.edu.ar
(R. Carelli), teodiano@ele.ufes.br (T. Bastos).

mobile robots in advanced interaction scenarios is expected to enable a new generation of service robots and healthcare applications [7].

Service robots are not only expected to navigate within the environment, but they also should interact with people. Basically, as service robots focus attention on humans, and considering that human behavior is difficult to model or predict, it is interesting to achieve tracking systems with high quality and precision in order to assess the human motion using a robot. This allows a more natural human–robot interaction.

The development of wearable systems allows very important improvements to human motion detection. The contribution of this paper can be summarized in two aspects: a new human–robot interaction strategy based on the human gait by combining data from a wearable IMU (Inertial Measurement Unit) and an onboard Laser Range Finder (LRF), and a new robot–human controller for tracking in front with an experimental validation of the controller performance. The proposed controller was evaluated with an eight-shaped curve, showing stability even with changes in the human path and keeping a continuous following in front of the human during real experiments.

The next sections present some important remarks considering human tracking systems, control strategies to human–robot interaction and some considerations related to human gait that will be described in this work.

1.1. Human tracking by mobile robots

As previously discussed, human tracking is essential for mobile service robots and human–robot interaction applications. There are a variety of approaches; most of them employ both visual tracking and/or Laser Range Finder (LRF) devices [8–11]. However, when the robot is tracking a person in outdoors, visual measurement errors are expected to increase. For this reason, some researches apply LRF human tracking [12–16]. The use of LRF is advantageous because it is robust with respect to illumination changes in the environment. Additionally, it is important to mention that wearable IMU sensors are appearing in this field, offering the possibility of combining human tracking with human gesture detection and body posture estimation [17–21].

One common way for human detection by LRF is scanning legs. In this case, apart from tracking the position of the human in relation to the robot, other important human gait information can be obtained allowing a more adaptable human–robot interaction. Step length, cadence, velocities, legs orientation, and gait phases (stance and swing) are some examples of information that could be obtained from tracking the human legs. Nevertheless, it is important to observe that the tracking system has to deal with specific situations, such as clothing. Therefore the use of some clothes that fully covers human's legs, such as long skirts, is a limitation and is not considered in this work.

A basic technique for leg detection uses the acquired data from LRF, defining the measurement range that violates the static environment assumption to determine leg position [11]. Other approaches make use of specific geometrical shapes to determine leg position. In [12], circle shapes are suggested to extract leg data. In [13] and [14], the approach is inductive on the basis of sufficient measurements without specific assumptions of shapes and also exploiting a human walking model. Such approaches do not present an exhaustive experimental evaluation and do not explain how the performance of the detection algorithm is affected when the legs cannot be detected. It is important to mention that leg obstruction is very common in circle or curved paths, when one leg can be placed behind the other from the sensor point-of-view.

Another proposal suggests the use of LRF for human torso tracking [15,16]. An advantage of this approach is that the scanned data presents smaller variations caused by the oscillatory movements during the human's gait, and obstruction and occlusion issues when performing curved paths do not represent a problem. As a disadvantage, human gait information (a fully modeled process) is not obtained and cannot be used as an extra input to the system. On the other hand, the works presented in [15,16] propose the estimation of body pose information using particle filters. However, the human tracking is not effective when detecting non-human objects with similar shape and width of human segments.

In this context, the use of wearable IMU sensors (already fully integrated in personal mobile devices) on the human's body may present important advantages eliminating the possibility of uncertain situations.

Some examples of wearable IMU sensors combined with tracking systems for gesture detection in indoor applications (environmental-robot interaction) can be found. In [17], an approach to detect movements of a person, and estimate of the human path using a wearable IMU is shown. In [18], a robot finds the human subject through onboard vision and identifies the activity he/she is performing by the use of two wearable IMU sensors placed to the subject's body.

Considering the combination of LRF and IMU sensors for human tracking, in [19], a method for combining kinematic measurements from LRF mounted on the robot and an IMU carried by the human is shown. A proposal to extract human velocity and position is also presented. However, that study does not provide any information regarding the validation of the proposed method. In [20], a study in which several robots were programmed to follow a person for the purpose of mapping a building for firefighters' rescue missions is presented. This sensor combination is employed to avoid the use of information obtained from artificial vision systems, such as cameras. In this case, the objective is to map the building for situations in which there is low visibility caused by fire. An IMU was used for mapping and locating the current position of a firefighter and, finally, providing the subject an exit path. Finally, a method for human motion capturing in large areas is described in [21], which shows a tracking approach that aims to provide globally aligned full body posture estimates by combining information from sensor on a mobile robot and multiple wearable IMU sensors attached to the human subject.

Summarizing, works found in the literature indicate a trend for future developments in the field of human tracking using mobile robots that rely on the integration of LRF and human motion capturing by means of wearable IMU sensors. This approach needs further investigation, and appropriate sensor integration algorithms have to be implemented, which is the main focus of this work.

1.2. Human following and mobile robot control

The use of control strategies for mobile robot following behind the human is a common approach in many works, such as [14,21]. Alternatively, there is another approach with the "side by side" behavior [22,23]. Recently, an alternative behavior was introduced in [16,24], where the mobile robot follows the human while positioned in front of him/her. Accompanying in front of a human is useful in many applications: if the robot carries tools, materials or merchandise to be dispensed, it is more natural and comfortable for the person to access the items if the robot is placed in front of him/her [24].

Specifically in [16], the authors developed one experiment with subjects walking or running along a straight line, and a mobile robot tracking and following the subject from behind. This experiment has indicated that a robot moving behind the human causes the human to always pay attention to its motion. Therefore,
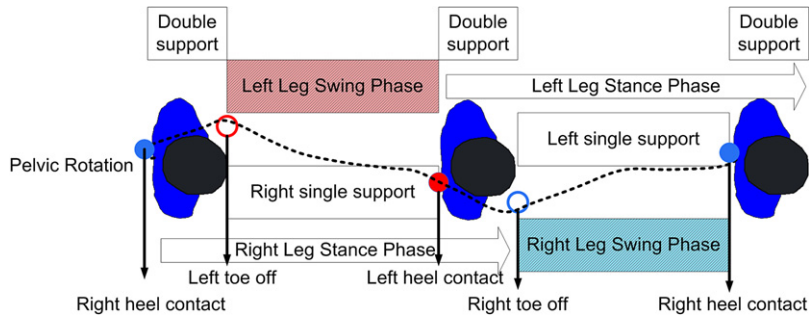
Fig. 1. Gait phases and pelvic rotations on the transverse plane.

when the robot accompanies a human while staying in his/her field-of-view, this makes the human feels more comfortable.

Indeed, there are fundamental differences in motion between conventional wheeled mobile robots and humans. A possible solution is to use the control system to absorb this kinematic difference between human and the mobile robot locomotion. In [25,26], a virtual spring model is used. This method is derived from the assumption that the human target and the mobile robot are connected by a virtual spring. The input velocity to a mobile robot is generated on the basis of an elastic force of a virtual spring, and this proposal absorbs the gap between the human and the mobile robot motion.

Another solution is the presumption based on the detailed analysis that human walking is included into the control. In this work, the goal is to develop a natural robot following in front of the human interaction strategy based on the human gait model. The method presented in the following sections proposes a human–robot interaction strategy using the integration of a LRF tracking of human legs with wearable IMU sensors for capturing the human movement during the gait. This work also presents detailed information regarding the implementation and experimental validation of the proposed interaction scheme.

1.3. Brief considerations regarding the human gait

The human gait process starts as a nerve impulse in the central nervous system and ends with the generation of the ground reaction forces. The gait cycle is defined as the time interval between two successive occurrences of one of the repetitive events of walking. Fig. 1 presents the gait cycle divided into two phases; stance and swing for each leg. Analyzing only the right leg, leg stance is the entire period in which the right foot is in contact with the ground. This phase is subdivided into three intervals, such as: two double supports and one right single support. Both the start and the end of stance involve a period of bilateral foot contact with the floor (double support). Right single support begins when the left foot is lifted for swing (Left Leg Swing Phase). Alternatively, during the right leg swing phase, the right foot is in the air and the right leg is swinging through preparation for the next foot strike [27].

During walking the body functionally divides itself into passenger and motor units. The head, neck, trunk and arms are grouped as a passenger unit and the two lower limbs and pelvis are the motor system. The hip represents the junction between the passenger and the motor units. It provides three-dimensional motion with specific muscle control for each direction of activity. During the stance, the primary role of the hip muscles is stabilization of the superimposed trunk. During swing, limb control is the objective. During each stride the pelvis moves in all three directions. The site of action is the supporting of the hip joint. Consequently, the greatest amount of motion occurs at the pelvis. All motions follow small
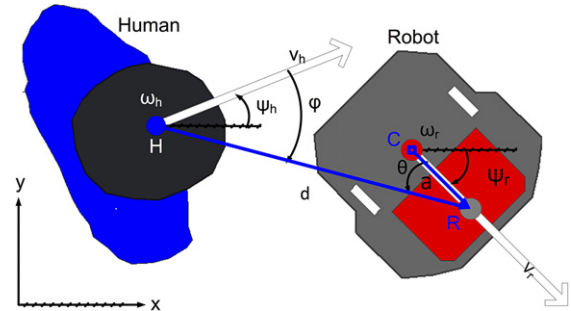

Fig. 2. Model for the human–robot interaction.

arcs, representing a continuum of postural change [28]. The transverse plane of pelvic rotation [29] is also shown in Fig. 1.

This work is organized as follows. Section 2 describes the methodology of this work, where the human–robot interaction, the parameter estimation, the robot and sensor integration setup and the parameter detection algorithm are presented. Section 3 describes the experimental study, with three different experiments in order to verify the accuracy of the human–robot interaction parameters detection. Section 4 shows the experimental results on the human–robot controller, as well as the discussion about them. Finally, conclusions and future work are presented in Section 5.

2. Material and methods

The approach presented in this work is focused on tracking the normal human gait in order to get a more natural robot following in front of the human. This way, the work was carried out in four stages. First, the definition of the kinematic model of human–robot interaction and the control system were developed. Second, a method for parameter estimation based on the human gait is presented. Third, the robot and sensor integration setup is introduced. Finally, the description of the algorithm for parameters detection is presented.

2.1. Human–robot interaction strategy

A model for the human–robot interaction was developed, which is shown in Fig. 2, where the variables and the parameters are: human linear velocity (v_h), human angular velocity (ω_h), human orientation (ψ_h), robot linear velocity (v_r), robot angular velocity (ω_r), robot orientation (ψ_r). Some interaction parameters were defined, such as the angle φ between v_h and the human–robot segment $\overline{RH}$, the angle θ between v_r and the $\overline{RH}$ segment, and the $\overline{RH}$ length (d). Finally, the parameter a defines the distance between the reference point (R) and the robot center of rotation (C).

The control system is based on the inverse kinematics. The variables to be controlled are the angle φ and the distance d. The
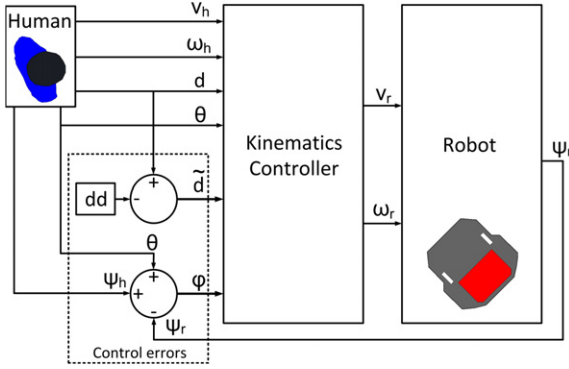
Fig. 3. Block diagram of the proposed controller.

control objective is to achieve a desired human–robot distance dd and angle φ to converge asymptotically to zero. Eq. (1) shows the direct kinematics of the robot, where $\tilde{d} = d - dd$ is the difference between the desired and the measured distances, and v_r and ω_r represent the linear and angular velocity to the robot. As it can be observed in Fig. 2, $\dot{\tilde{d}}$ depends not only on v_h and v_r, but also on ω_r, due to the fact that the reference point (R) is not located at the robot rotation center (C). Therefore, when ω_r is modified, it results in a d change. Finally $\dot{\varphi}$ depends on v_h, v_r, ω_h and ω_r as expected.

$$\begin{pmatrix} \dot{\tilde{d}} \\ \dot{\varphi} \end{pmatrix} = \begin{pmatrix} \cos\theta & -a\sin\theta \\ -\dfrac{\sin\theta}{d} & -a\dfrac{\cos\theta}{d} \end{pmatrix} \overbrace{\begin{pmatrix} v_r \\ \omega_r \end{pmatrix}}^{u} + \begin{pmatrix} -v_h\cos\varphi \\ \omega_h + v_h\dfrac{\sin\varphi}{d} \end{pmatrix}. \qquad (1)$$

From this kinematics model, it is possible to calculate the inverse kinematics controller shown in Eqs. (2) and (3), which are the components of the u-vector.

$$\begin{aligned} v_r = & \cos\theta \left[-k_d\,\tilde{d} + v_h\cos\varphi \right] \\ & - d\sin\theta \left[-k_\varphi\varphi - \omega_h - \dfrac{v_h}{d}\sin\varphi \right] \end{aligned} \qquad (2)$$

$$\begin{aligned} \omega_r = & -\dfrac{\sin\theta}{d} \left[-k_d\,\tilde{d} + v_h\cos\varphi \right] \\ & - \dfrac{d}{a}\cos\theta \left[-k_\varphi\varphi - \omega_h - \dfrac{v_h}{d}\sin\varphi \right]. \end{aligned} \qquad (3)$$

The parameters to be adjusted are the controller positive gains k_d, k_φ.

In this work, no dynamics effects are assumed. This assumption is based on the fact that human gait consists of slow movements, especially in human–robot interaction scenarios, as previously observed in [30]. However, if it becomes necessary, a dynamic compensator could be integrated into the control scheme. This compensator could be obtained from an identification process [31]

and used in series with the kinematic controller [32,33]. On the other hand, the human dynamics are not considered. However the human kinematics is here used as an input to the control law. In this context, the commands are given directly to the robot to follow the human.

In this kinematic approach, using the proposed control law and assuming a perfect velocity tracking by the robot, the control errors $\tilde{d}$ and φ converge to zero. This conclusion becomes evident after substituting (2) and (3) into (1), thus obtaining

$$\begin{pmatrix} \dot{\tilde{d}} \\ \dot{\varphi} \end{pmatrix} = \begin{pmatrix} -k_d\,\tilde{d} \\ -k_\varphi\varphi \end{pmatrix}. \qquad (4)$$

Therefore, the control system is exponentially asymptotically stable (5).

$$\begin{aligned} \tilde{d}(t) &= \tilde{d}(0)e^{-k_d t} \\ \varphi(t) &= \varphi(0)e^{-k_\varphi t}. \end{aligned} \qquad (5)$$

The control structure here proposed is shown in Fig. 3, where the control errors are $\tilde{d}$ and φ. The error φ can be obtained as a function of θ, ψ_h and ψ_r (Fig. 2). The other inputs to the controller are v_h, ω_h, d and θ. The output of the controller is the control actions v_r and ω_r.

In the approach presented in this work, human walking information and spatio-temporal gait parameters are included into the strategy for the estimation of the interaction parameters. Indeed, control inputs (set-points) are updated at each gait cycle. At the end of each gait cycle, controller outputs are calculated and sent to the robot. At the same time, the new parameter detection process starts with the next gait cycle. In the next section, the estimation of the control parameters will be explained with more details.

2.2. Parameter estimation

Control parameter estimation is based on the combination of LRF and IMU sensors as previously commented. Legs position and orientation is obtained from the LRF measurements and the trunk motion is captured by an IMU sensor located on the human pelvis. An example of trunk motion during a normal gait cycle (GC) is depicted in Fig. 4 (dashed line). The method to obtain the parameters of the proposed model is as follows:

- Human linear velocity (v_h) is the rate of change of the position in each stride. Therefore, during the human walking, it is necessary to detect the beginning and the end of the gait cycle.
- Human angular velocity (ω_h) is the average angular velocity during each cycle gait. This velocity is measured in this approach from the rate change of the pelvic rotation.
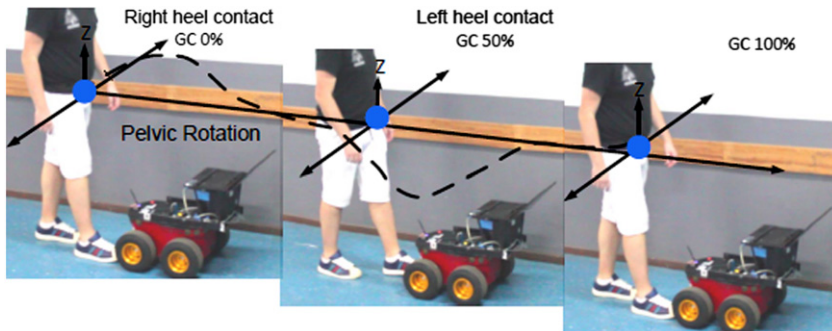- Human orientation (ψ_h) is the average of the pelvic rotation during each cycle gait.

Fig. 4. External and internal measurement of the gait with the robot following the human in front.
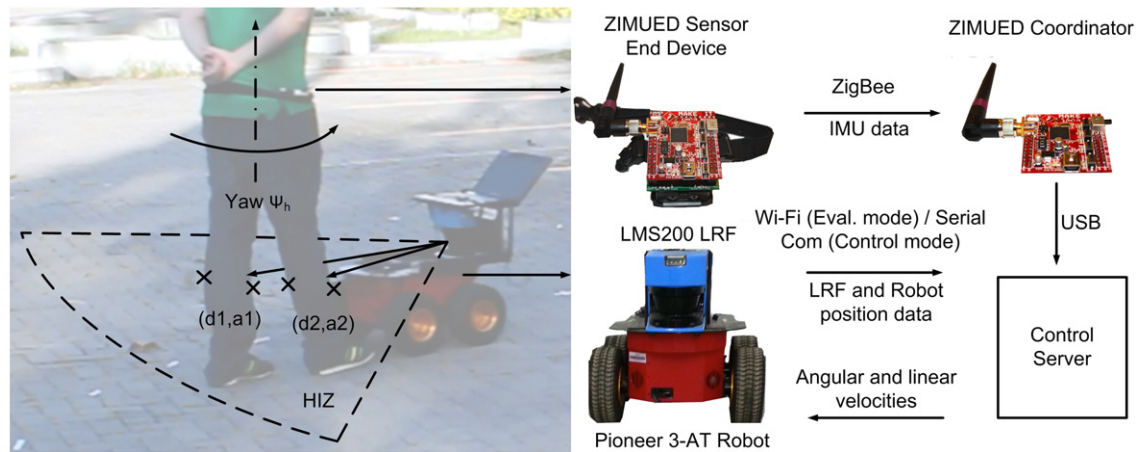
Fig. 5. Robot and sensor integration setup.

- Robot orientation (ψ_r) is measured by the robot odometry sensors. However, an onboard IMU sensor can be used in order to get a more accurate measurement.
- θ represents the human orientation in relation to the robot. In order to get an accurate measurement despite the human is walking, it should be measured when both legs have equal distance from the robot (d, obtained with the LRF sensor), and at the same time, the pelvic rotation is near to zero (Fig. 4).
- φ represents the difference in orientation between v_h orientation vector and the human–robot segment $\overline{RH}$ (Fig. 2). φ is also equal to $\theta - \psi_r + \psi_h$ (Fig. 3). This angle is only defined if the magnitude of the v_h is greater than zero.

2.3. Robot and sensor system setup

A mobile robot Pioneer 3-AT [34] was used in this work. The robot has an onboard computer with a Wi-Fi link, which receives the robot state (x, y, ψ_r) as well as the control information, such as angular and linear velocities, as shown in Fig. 5.

The maximum linear velocity is set to 0.7 m/s and the maximum angular velocity is set to 140°/s. It can also be seen in Fig. 5 a SICK LMS-200 LRF [35], which is mounted at the legs height level, with an angular resolution of 1°.

The IMU sensor used to measure the human pelvic motion was developed in a previous research [36,37], which is a wearable ZigBee IMU called ZIMUED. This sensor node is capable of sending data such as 3D accelerations, 3D angular velocities, 3D magnetic information and orientation data (roll, pitch and yaw) through ZigBee to the ZIMUED Coordinator. This sensor is attached to the human pelvis as shown in Fig. 5.

The robot and sensor system integration setup has two possible configurations. The first one is the evaluation of the human-interaction parameters, where a remote computer receives the LRF data and robot orientation through WI-FI link. In this mode, the controller is not executed, but it is useful to analyze the performance of the parameters detection algorithm. The second mode is the *control mode*, in which the onboard computer receives the sensor information to execute the controller. A ZIMUED coordinator is linked by ZigBee connection with an IMU sensor on the human. In the same way, the coordinator sends the human IMU data to a USB connection with the computer for both configurations. LRF and robot states are sampled every 100 ms and the ZIMUED sensor at every 20 ms. At the same time, the robot is able to receive the control commands such as angular and linear velocities to be performed.

In the control mode, the main program receives IMU data every 20 ms. This packet defines the main clock of the detection algorithm. The performance of the communication was evaluated in [36]. With the conditions used in this setup, the wireless communication does not present loss in data packets. However, if the controller is executing and suddenly the ZigBee communication is broken, the detection algorithm is blocked, and an internal timer is started. If no packets are received within 100 ms, the robot is automatically stopped for a secure operation.

The leg detection approach presented in this work combines techniques presented in [8,38], which is split into four basic tasks: LRF data pre-processing, transitions detections, pattern's extraction and estimation of legs' coordinates. In the pre-processing phase, the delimitation of the HIZ (Human Interaction Zone) is performed (Fig. 5). Then, the laser scanning data are used to identify transitions.

The legs positions are calculated in polar coordinates (Fig. 5). The general process is based on the differences between two transition events that define a leg pattern (x-marks on Fig. 5). After that, both distance and angle measurements are calculated in relation to the middle point of each leg. In Fig. 5, (d1, a1) and (d2, a2), respectively, represent the polar coordinates of left and right legs.

The angle range of the HIZ is restricted from −60° to 60°, and the scanning distance from the LRF is limited up to 2 m. On this range, the human can walk freely but the legs cannot present any occlusion. When one leg cannot be detected as a cause of screening by the other leg, the algorithm calculates the human distance with the only one leg detected. Finally, in the case the human leaves the HIZ, the robot is automatically stopped.

2.4. Parameters detection algorithm

The parameter estimation here proposed is based on the leg detection from the LRF and pelvic rotations (see Fig. 4) obtained from the IMU sensor (Fig. 5). This signal is represented by the yaw orientation. The velocity of this orientation is periodical due to the periodicity of the human gait, making this signal suitable to synchronize the parameter estimation every gait cycle. In Fig. 5, the signals of the pelvic motion and laser detection of the Right and Left Legs (RL and LL) distances are shown. These measurements were obtained through experiments with a person walking towards the LRF sensor.

In Fig. 6a the pelvic angular velocity obtained from the Z axis gyroscope signal is shown. The zero crossing points are marked with a circle and square at every gait cycle. Fig. 6b shows the square mark representing the maximum pelvic orientation (they happen after the right heel contacts the ground). The circle mark represents the minimum pelvic orientation (it happens after the left heel contact). At the same time, these events are presented in the RL and
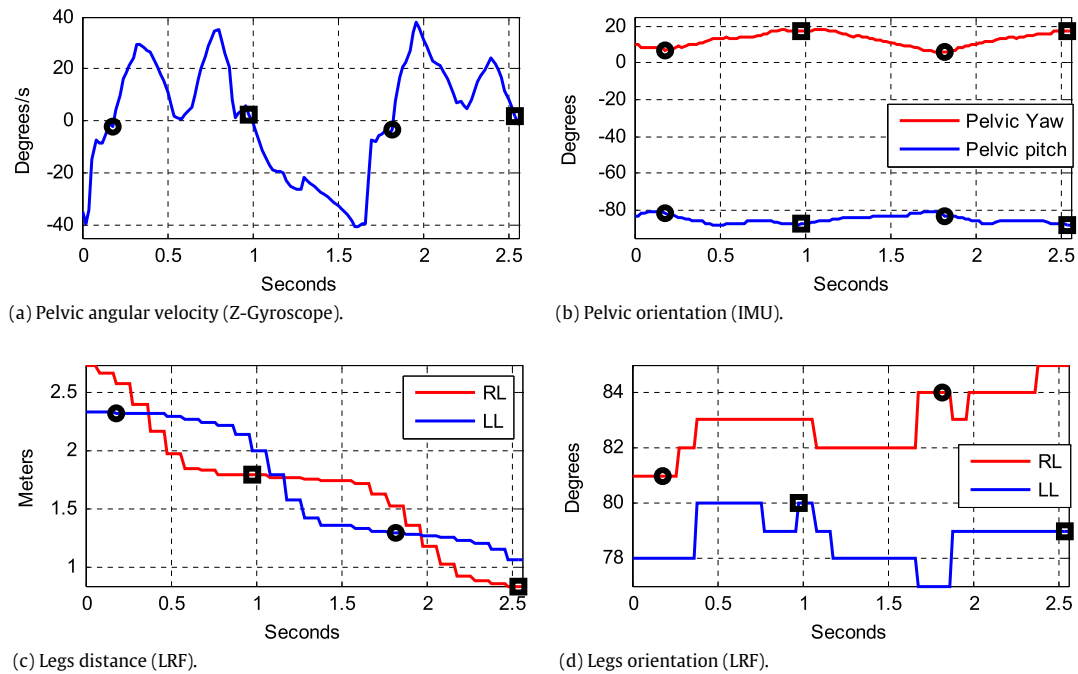
(a) Pelvic angular velocity (Z-Gyroscope).

(b) Pelvic orientation (IMU).

(c) Legs distance (LRF).

(d) Legs orientation (LRF).

Fig. 6. Detection of zero crossing points over pelvic angular velocity.

LL distances and orientation trajectories respectively (Fig. 6c,d). The parameter detection algorithm is performed as follows:

- Human linear velocity (v_h). This parameter is updated at each step. The interval between the last two zero crossing points represents the step time. The step length is the distance performed in one step. It is obtained from the maximum distance between right and left legs during the step time. The magnitude of v_h is the step length divided by the step time. Due to the fact that the robot linear velocity limit is 0.7 m/s, it is recommended to the human not to exceed this limit.

- Human angular velocity (ω_h). This parameter is calculated at each stride. This is the average of all values of angular velocity (from Z-Gyroscope) during one stride. Therefore, if the human is walking straight, the oscillatory form of the gait ω_h will be close to zero (see Fig. 5). Although the robot angular velocity is limited to 140°/s, this does not cause any problem as the human does not achieve such high angular speed during normal interaction.

- Human orientation (ψ_h). This parameter is calculated at each stride. This is the average of all values of the pelvic orientation (from pelvic yaw) during one stride. The range of this angle is between −180° and 180°.

- Robot orientation (ψ_r). This orientation is measured by the robot odometry at each step. The range of this angle is between −180° and 180°. Despite the odometry is the most widely used method to obtain the robot position, there are well known errors from this measurement method [39]. A more accurate measurement could be obtained by using an IMU mounted on the robot. The use of an IMU is especially important during experiments that last several minutes, as the cumulative odometry errors are more significant.

- θ angle and human–robot distance (d). θ is the average between right and left legs orientation from the LRF legs detection. The range of this angle is restricted between −60° and 60°. This is calculated when both legs have the same distance (crossing point); thus, the human–robot distance is obtained. The range of this distance is limited up to 2 m.

- φ angle. This angle is calculated as $\theta - \psi_r + \psi_h$ at each stride.

3. Experimental study for validation of the estimation of interaction parameters

Three different experiments were developed in order to verify the accuracy in the detection of the human–robot interaction parameters with the proposed algorithm. In the first and second experiments, no motion was performed by the robot. The subject was asked to walk on a straight line following different paths marked on the floor to define specific angular parameters (θ, φ and ψ_h), the parameter v_h was defined during each test according to the human gait and compared with the estimated parameters.

In the third experiment, the robot is configured with specific linear (v_r) and angular (ω_r) velocities, and the human follows the robot keeping a constant distance. Human linear and angular velocities are estimated in a more dynamic scenario and are compared with the reference velocities performed by the robot.

The layout of the paths for the first experiment is shown in Fig. 7a. These paths, marked on the floor (black dashed lines), have different predefined θ angles with respect to the LRF reference: −20°, −15°, −10°, −5°, 0°, 5°, 10°, 15° and 20°. One volunteer was asked to walk on a straight line in the direction of the robot, performing three repetitions of each one of the proposed paths. The assumption was that both θ measured from LRF and ψ_h measured from the IMU should have the same value to the predefined angles during every path, as it can be observed in Fig. 7b. In this experiment φ angle is always equal to zero.

The layout of the paths proposed on the second experiment is shown in Fig. 8a. These paths marked on the floor (black dashed lines) are performed to evaluate the φ angle estimation based on the direct measurement of θ by the LRF. Thereby, despite the fact that the start points were the same of the first experiment, all paths are now parallel to each other. One volunteer was asked to perform three repetitions of the proposed paths. Then, every path is performed by the volunteer with the same linear velocity (v_h) orientation, as it can be observed in Fig. 8b. Therefore, the assumption in this experiment is that both θ and φ have the same magnitude and opposite signs. Each path was labeled (T1, T2, T3, T4, 0°, T5, T6, T7 and T8) as shown in Fig. 8b.
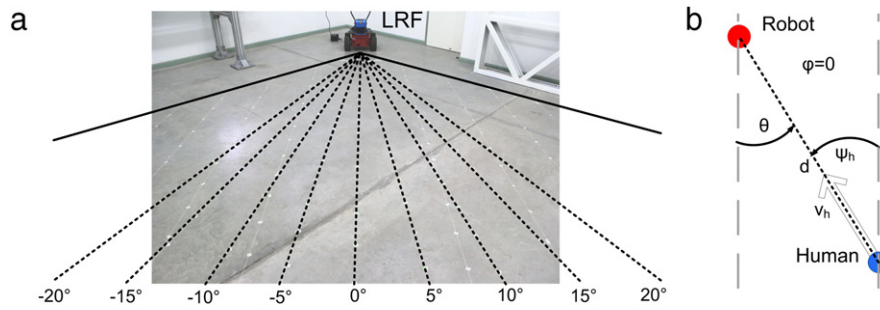
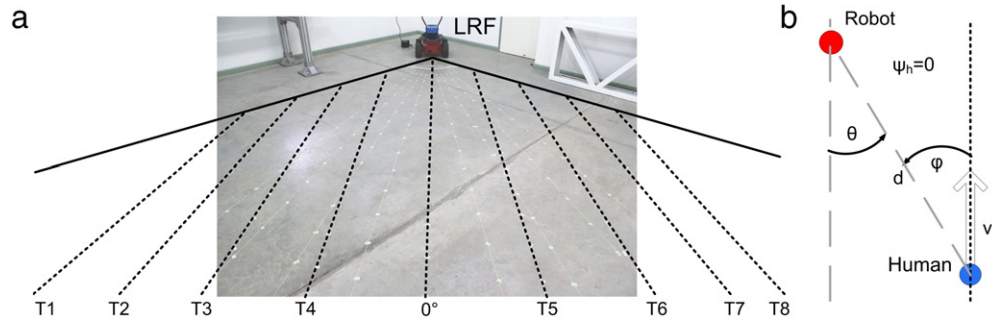**Fig. 7.** First experiment. (a) Proposed paths; (b) Interaction parameters.

Fig. 8. Second experiment. (a) Proposed paths; (b) Interaction parameters evaluated.
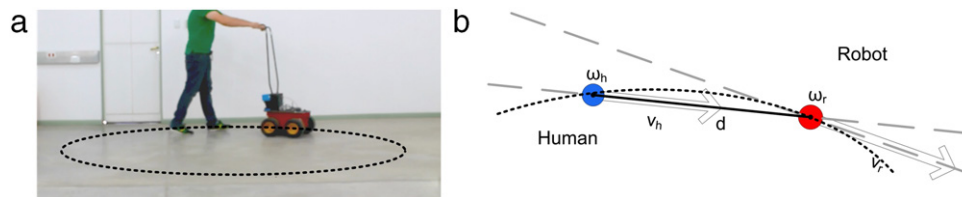

Fig. 9. Third experiment. (a) Paths layout and human location to perform the circle path; (b) Interaction parameters evaluated.

Additionally, in the first and second experiments, each test was performed with three predefined linear human velocities (v_h): 0.25, 0.5 and 0.75 m/s to assess the effect of different gait speeds on the estimation process. The selection of these velocities is based on past experience in human–robot interaction scenarios, such as carrying loads or in walker-assisted gait [30]. Thus, every path was marked with distance intervals (0.25, 0.5 and 0.75 m). In order to achieve the desired velocities, steps were performed following a sound indication produced at every second.

In the first and second experiments the human angular velocity is not evaluated. Therefore, to verify the estimation process of this parameter, a third experiment was performed with a circle-shaped path (Fig. 9). Thus, the robot was programmed to perform constant linear and angular velocities. The human was asked to maintain a constant distance while following the robot. To simplify this task, human hands were kept in contact with the robot as shown in Fig. 9a. The assumption in this experiment is that human angular and linear velocities will be approximately equal to the robot's velocities (Fig. 9b). Three circle-shaped trajectories with different constant linear and angular velocities were programmed: (i) 0.15 m/s and $-7°/s$; (ii) 0.25 m/s and $-11°/s$; and (iii) 0.30 m/s and $-14°/s$.

4. Experimental results

The results of the three experiments show the precision and variability of the human-interaction parameters estimation.

Section 4.1 presents the results of the experimental validation of the proposed methodology for the estimation of interaction parameters.

Once the procedure for the estimation of the interaction parameters are validated, the results of the experimentations with the proposed controller are presented in Section 4.2. First, a simulation is considered to demonstrate the expected behavior of the interaction strategy. Finally, the results of a final experiment are presented, showing the human-interaction parameter detection and the controller being executed, both in real-time, by the mobile robot embedded system.

4.1. Detection and estimation of human–robot interaction parameters

In the first experiment, θ and ψ_h estimation remain near the expected angle in every test. Fig. 10 shows a part of the measurements and estimated parameters performed in three predefined velocities ($v1 = 0.75$ m/s, $v2 = 0.50$ m/s and $v3 = 0.25$ m/s) in the -5 degrees path. IMU and LRF data (continuous signals) are presented along with the human linear velocities and angular parameters (discrete values) obtained in two foot strikes.

The angular velocities obtained from the gyroscope in the z-coordinate are shown in Fig. 10a. As expected from normal gait, there is an increase in pelvic rotation for greater linear velocities. The average of the angular velocity remains close to zero because the human is walking in a straight line. Pelvic yaw and pitch angles
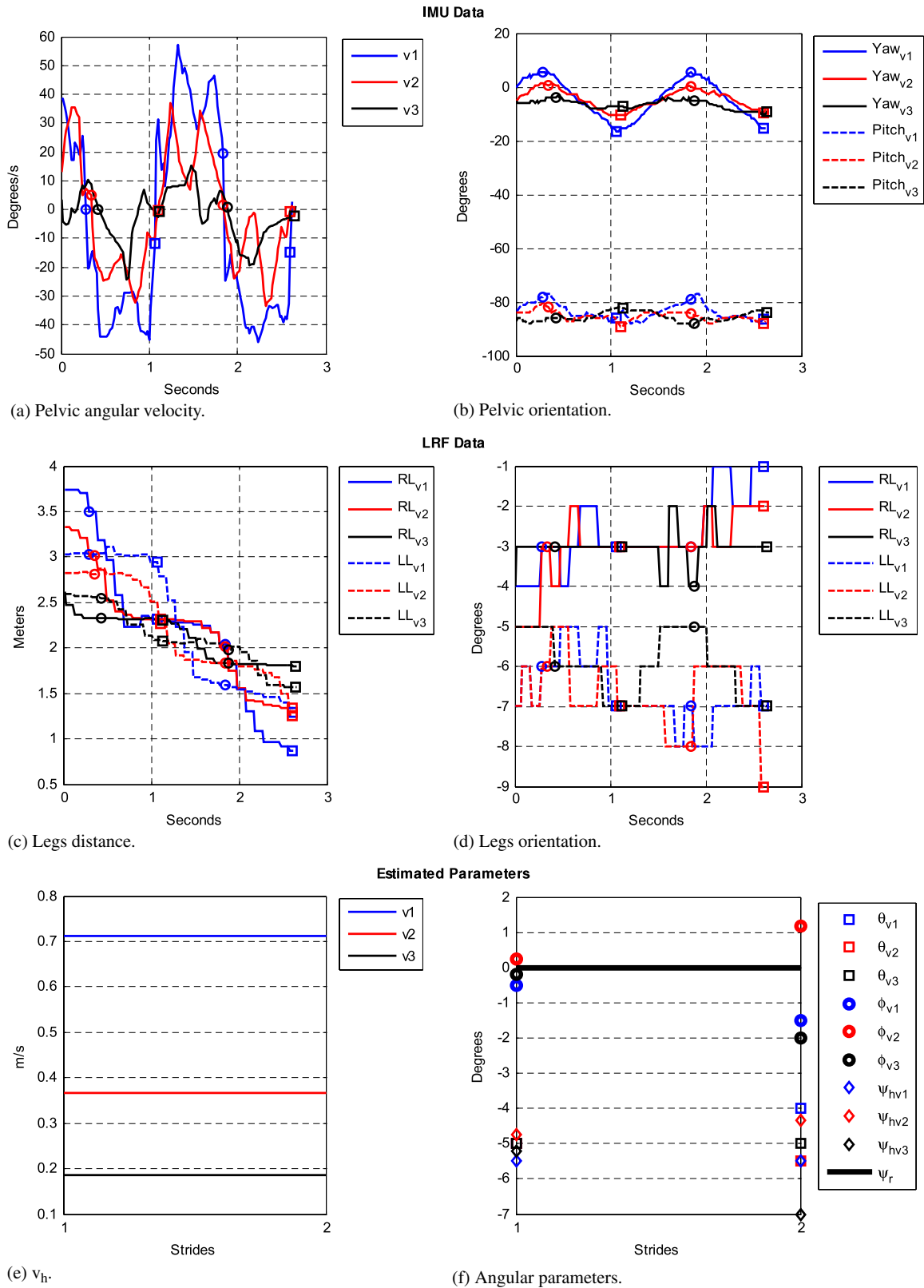
Fig. 10. Measurements and estimated parameters performed in the first experiment of the test of −5 degrees. (a) Pelvic angular velocities from z-axis gyroscope; (b) Pelvic orientation from IMU; (c) Legs distance curves from LRF detection; (d) Legs orientation curves from LRF detection; (e) Estimated v_h; (f) Estimated θ, ψ_h, φ and ψ_r angles.

are shown in Fig. 10b, where ψ_h is obtained from the yaw angle. It is also observed an increase in the oscillation amplitude with the increase of v_h.

The paths of the human legs obtained in these intervals are shown in Fig. 10c. As expected, length stride increases when v_h

increases. As the robot is not moving, the module of the slope of these curves is the actual v_h. The negative values of the slope indicate the decrease in the distance as the subject is walking towards the LRF. Although feet position (indication of the step length) were marked on the floor, the resolution of the step length
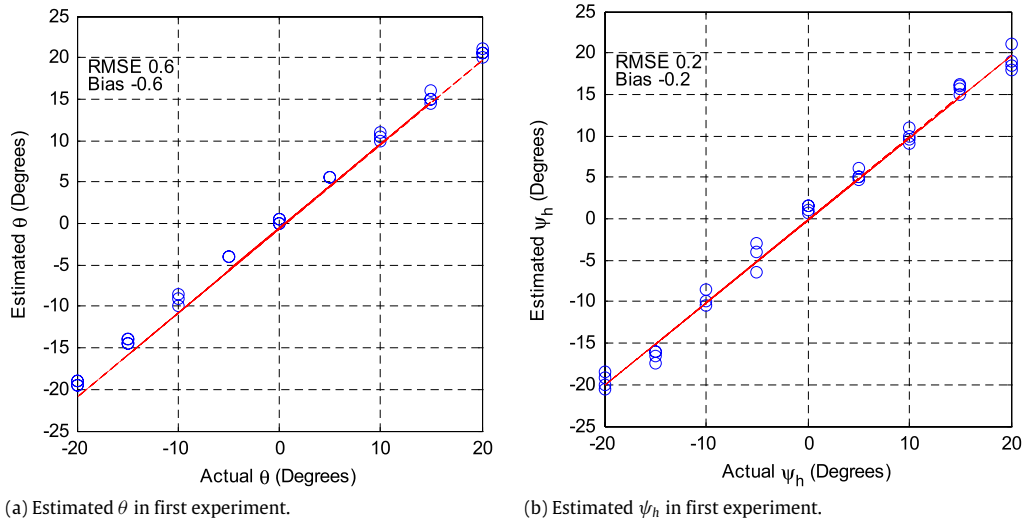
(a) Estimated θ in first experiment.

(b) Estimated ψ_h in first experiment.

Fig. 11. Estimated values of θ and ψ_h versus reference angles from the first experiment.

(a) Tests T1 T2 T3 T4 HLV 0.5 m/s.
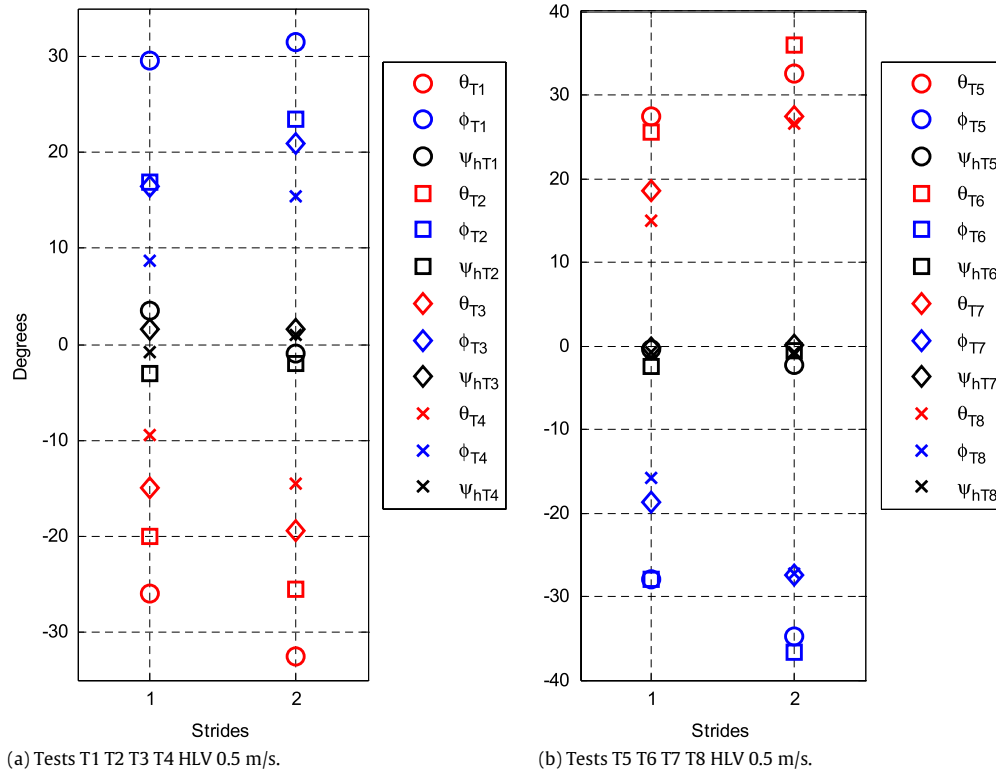

(b) Tests T5 T6 T7 T8 HLV 0.5 m/s.

Fig. 12. Estimated values of θ, φ and ψ_h from the second experiment.

measurements is defined by the shoe size, which is reflected on the error of the v_h estimation as shown in Fig. 10e.

The legs orientation obtained from the LRF detection is shown in Fig. 10d. Finally, the estimated angular parameters are shown in Fig. 10f. It can be observed that θ and ψ_h angles were close to the expected −5 degrees. Also, the φ angle is close to zero as proposed in this experiment.

From the first experiment, all estimated values of θ and ψ_h for different v_h were grouped and compared with the path angle (reference value). In the estimations of θ (Fig. 11a), the RMSE was 0.6° and the bias was −0.6°. The values obtained for the errors seem to remain constant in all experiments. This could be caused by a misalignment of the LFR sensor during the experimental setup. Regarding the estimations of ψ_h (Fig. 11b), the RMSE was 0.2° and

the bias was −0.2°. Despite of the continuous oscillation of the pelvis during walking, ψ_h estimation was precise and unbiased, showing also repeatability with changes of v_h.

Considering the second experiment, Fig. 12 shows the angular parameters during different tests in a single stride. It is possible to see that ψ_h remains close to zero, and θ and φ remain close to a same magnitude with opposite signs, such as expected.

From the first and second experiments, v_h average errors (RMSE) of all tests were grouped in Fig. 13a. The estimation of the error for 0.25, 0.50 and 0.75 remains under 0.15 m/s. Although this is high in comparison with the desired/performed speed, it is important to mention that errors can be caused by a misplacement of the feet in two consecutive steps. To illustrate this, one could imagine the situation in which the human steps the line with the
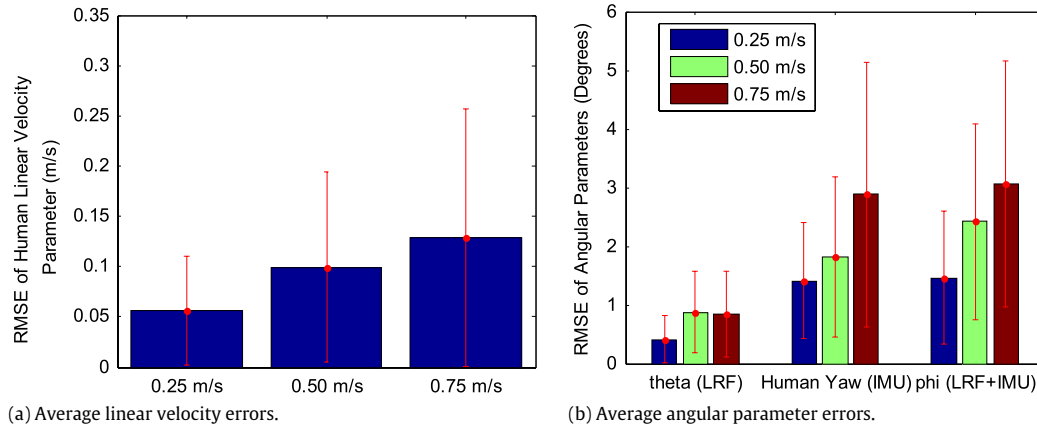
Fig. 13. Average errors (RMSE value) in estimation of v_h for 0.25, 0.50 and 0.75 m/s. (a) Linear velocity estimated errors; (b) θ, ψ_h and φ errors with the different velocities.

Table 1
Error in linear and angular velocities estimation for the third experiment.

Actual v_h (m/s)	Actual ω_h (°/s)	Estimated v_h (m/s)	Estimated ω_h (°/s)	Error v_h (%)	Error ω_h (%)
0.15	−7	0.149	−6.6	1%	5%
0.25	−11	0.253	−10.4	−1%	5%
0.3	−14	0.311	−13.2	−4%	6%

toe on a step and with the heel on the consecutive one. Considering that the foot size is of similar magnitude of the step lengths, errors with the presented magnitude are expected in these experiments.

Additionally, the errors of the angular parameters (Fig. 13b) remain close to 3°. The error of θ is considerably smaller (around 1°) due to the direct measurement of this parameter using the LRF, which presents high resolution.

In the third experiment, the robot follows constant angular and linear velocities describing a circle-shaped path. Fig. 14 shows a part of the measurements and the estimated parameters for the robot trajectory performed for linear velocity of 0.3 m/s and angular velocity of −14°/s.

The angular velocities obtained from the gyroscope in the z-coordinate are shown in Fig. 14a. Due to the performed circle path, the estimated ω_h remains close to −14°/s as expected (Fig. 14f). This measurement can also be observed in the tendency of the pelvic orientation values shown in Fig. 14b.

The position and orientation of the human legs obtained in this interval are shown in Fig. 14c,d, respectively. Due to the fact that the LRF and the legs are moving at the same time, it can be observed that these signals present a constant mean value. The v_h estimation is shown in Fig. 14e and remains close to the expected 0.3 m/s. During the tests, the human was following the robot. This can be observed through the pattern of the ψ_h and ψ_r angles in Fig. 14g. As a result of that, θ and φ are shown in Fig. 14h.

Table 1 shows the summary of the actual and estimated linear and angular velocities in the third experiment. The linear velocity error corresponds to the previous analysis, and the angular velocity error remains close 1°/s, which is acceptable in this kind of interaction strategy.

4.2. Controller evaluation

Fig. 15 shows a simulation of the proposed controller. The blue line in Fig. 15a represents the human path performing an eight-shaped curve (input to controller), and the red line is the path performed by the robot, following the human (controller output).

This simulation shows the stability of the controller even with sharp curves performed by the human. It can be observed how the

θ angle is close 30° (Fig. 15b) making a turn, and φ is kept less than 1° (Fig. 15c). Therefore, the proposed controller is expected to keep the robot continuously "following in front" of the human.

To evaluate the effectiveness of the controller and the parameter detection system, a final experiment with the robot following the human in front of the human was conducted, in which a volunteer performed the eight-shaped path shown in Fig. 16. During the execution of turns the robot follows the humans on the external side when he/she is making a curve (Fig. 15a). The human path and the expected robot's path (solid line) can be observed in Fig. 16. It is also shown in Fig. 16 the start and the end marks of the human path; the human walks in a straight line before entering the eight-shaped curve. It is noteworthy that the eight-shaped curve is analyzed in three phases: first, a semicircle path (human turning left); second, a circle path (human turning right); and third, a last semicircle path (human turning left). This way, it is possible to analyze the performance of the controller in straight lines and in curved paths.

Fig. 17 shows the IMU and LRF sensor data obtained during the proposed experiment. Although there are periodic (and tridimensional) oscillations of the pelvis during the gait and considering that the locomotion was performed in an eight-shaped path, the robot kept a continuous and stable orientation while following, such as shown by ψ_r (gray line in Fig. 17a).

Fig. 17b shows the raw signal obtained from the gyroscope placed on the human pelvis (gray line) and the filtered signal (black line). A second order Butterworth low-pass filter (cutoff frequency of 1 Hz) was used to reject high frequency components that are not associated to the gait cadence. As it can be seen, no significant delay was observed in this application.

The legs detection was adequate during the whole experiment as depicted in Fig. 17c (angle detection) and Fig. 17d (distance detection). The values of angular positions of the legs, measured from the robot, were in the range between −40° and 40° (Fig. 17c). These bounds belong to the range of detection previously defined [−60°, 60°]. In this experiment, the maximum interaction distance was set to 2 m and the desired distance dd (Section 2.1) was set to 0.9 m. Accordingly, the legs distance measurements were between 0.4 and 1.2 m during the whole the experiment (Fig. 17d).

Fig. 18 shows snapshots of different instants of the experiment illustrated in Fig. 16. It lasted about 80 s. From the beginning and up to the fifteenth second, the human walked in a straight line (Fig. 18a). After that, the human began to turn left (ψ_h in Fig. 17a) entering the eight-shaped path. The first semicircle is performed up to about the 30th s (Fig. 18b). The human orientation increased positively in this interval (Fig. 17a), indicating that he was turning left. The orientation of the legs (LRF data) decreased to 0° (Fig. 17c)
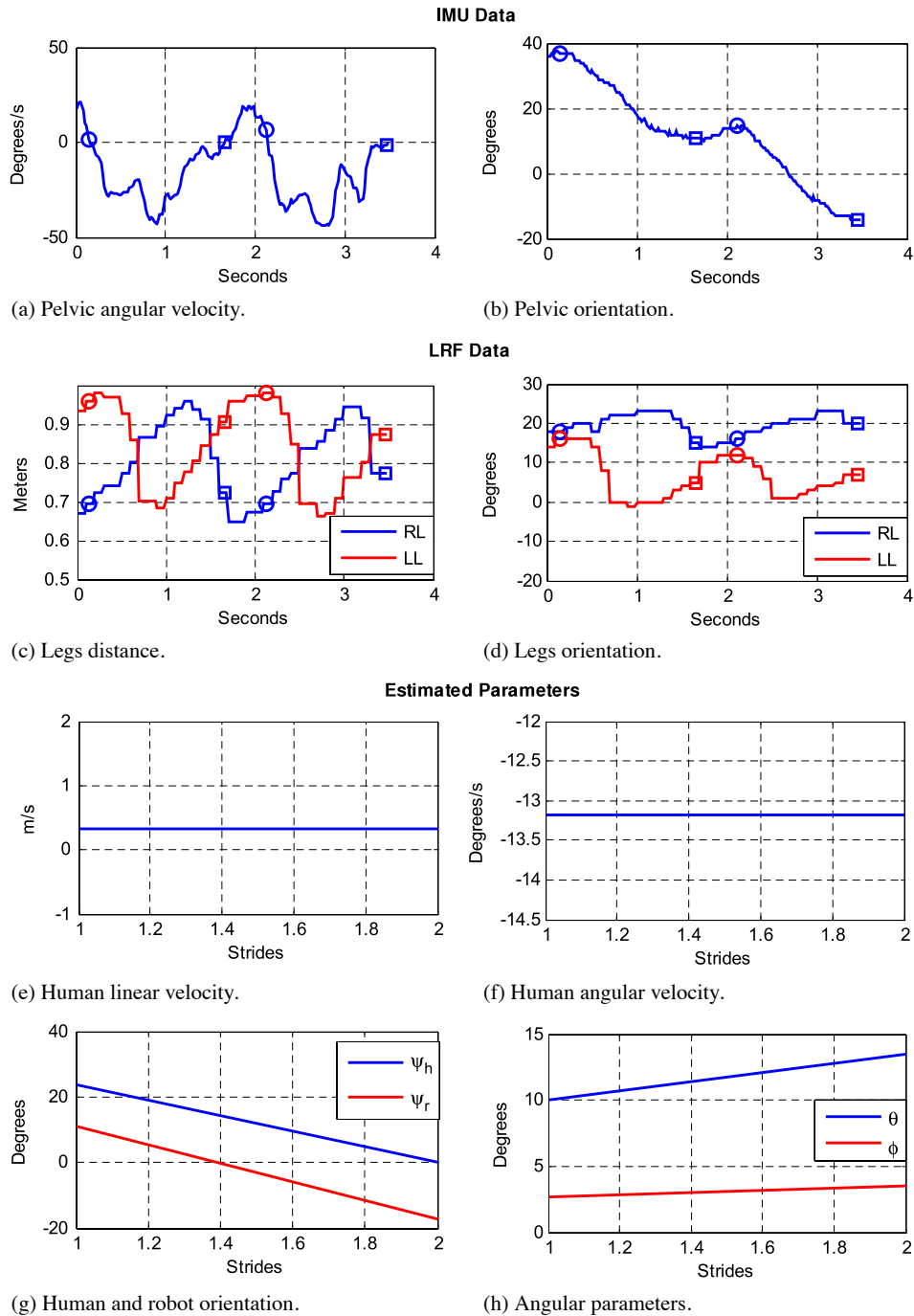
Fig. 14. Measurements and estimated parameters for v_h 0.3 m/s and $\omega_h - 14°/s$ from the first experiment. (a) Pelvic angular velocity from z-axis gyroscope; (b) Pelvic orientation from the IMU; (c) Legs distance curves from LRF detection; (d) Legs orientation curves from LRF detection; (e) Estimated v_h; (f) Estimated ω_h; (g) Estimated ψ_h and ψ_r; (h) Estimated θ and φ angles.

before finishing the first semicircle as the human starts planning the next circle (Fig. 18c).

This circle is completed before the 60th s (Fig. 18e). In this interval, the human orientation decreases constantly, as expected (see Fig. 17a), indicating that the he is turning right. After that, the angular positions of the leg become 0° again (Fig. 17c) in order to perform the last semicircle (Fig. 18e).

Finally, the human is back at the beginning of the eight-shaped curve (Fig. 18f). ψ_h and ψ_r angles are close to 0° again, as expected (Fig. 17a).

As aforementioned, all control parameters are detected in every gait cycle. Some of them are updated at every step while others are updated at every stride. However the controller variable update is

executed at every step. In the case that human does not perform another step, for example, when the human suddenly stops, the parameters are calculated at every second. Finally, Fig. 19 shows all control data recorded during the proposed experiment. The parameters estimation algorithm detects approximately 100 steps from the human in the execution of the proposed path.

In Fig. 19a, from the beginning and up to almost the step number 20, the human was walking in a straight line, as ψ_h, ψ_r and θ remains close to 0° (Fig. 19a). This way, φ (control error) remains close to 0°, as well. However, $\tilde{d}$ remains near -0.3 m (Fig. 19b). As a result of this, the control action $v_r(C)$ and the robot's actual speed $v_r(R)$ follow v_h with a maximum value of approximately 0.3 m/s
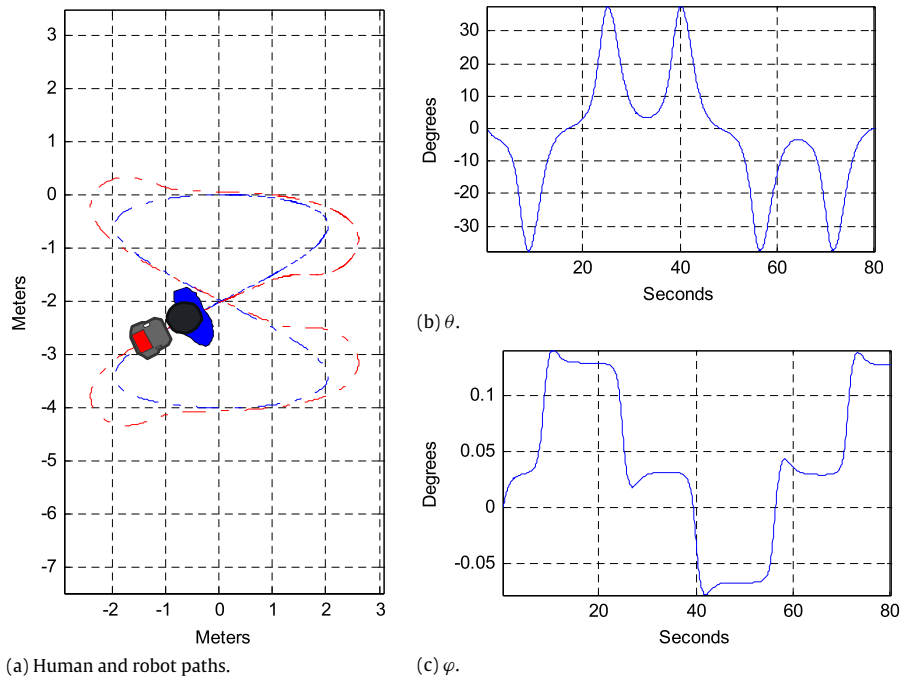
Fig. 15. Controller simulation. (a) Eight-shaped human path (blue dashed line), and the path of the robot following in front (red dashed line); (b) θ; and (c) φ responses. (For interpretation of the references to color in this figure legend, the reader is referred to the web version of this article.)

Fig. 16. Human path (dashed line) in an experiment performing an eight-shaped curve.

(Fig. 19c). Furthermore, the control action $\omega_r(C)$ and the measured velocity $\omega_r(R)$ remain close to 0°/s (Fig. 19d), as expected.

After the step number 20, the eight-shaped curve starts. From Fig. 19a ψ_r follows ψ_h continuously, θ is positive when the human is turning left and negative when the human is turning right, and φ remains close to 0°, as expected.

From Fig. 19b, $\tilde{d}$ was negative in most of the experiment. This indicates that the human walks forwards and the controller tries to reach the desired distance (0.9 m). From Fig. 19c, v_h was always lower than 0.5 m/s, however the control action, $v_h(C)$, reaches the robot's maximum forward speed (0.7 m/s) and also sometimes the backward speed limit (−0.7 m/s). The controller tries to bring the control errors to 0. $v_h(R)$ is delayed with respect to $v_h(C)$ due to robot dynamics, but this delay does not significantly affect the performance of the controller response with this experiment conditions. From Fig. 19d, $\omega_r(C)$ and $\omega_r(R)$ have adequate tracking
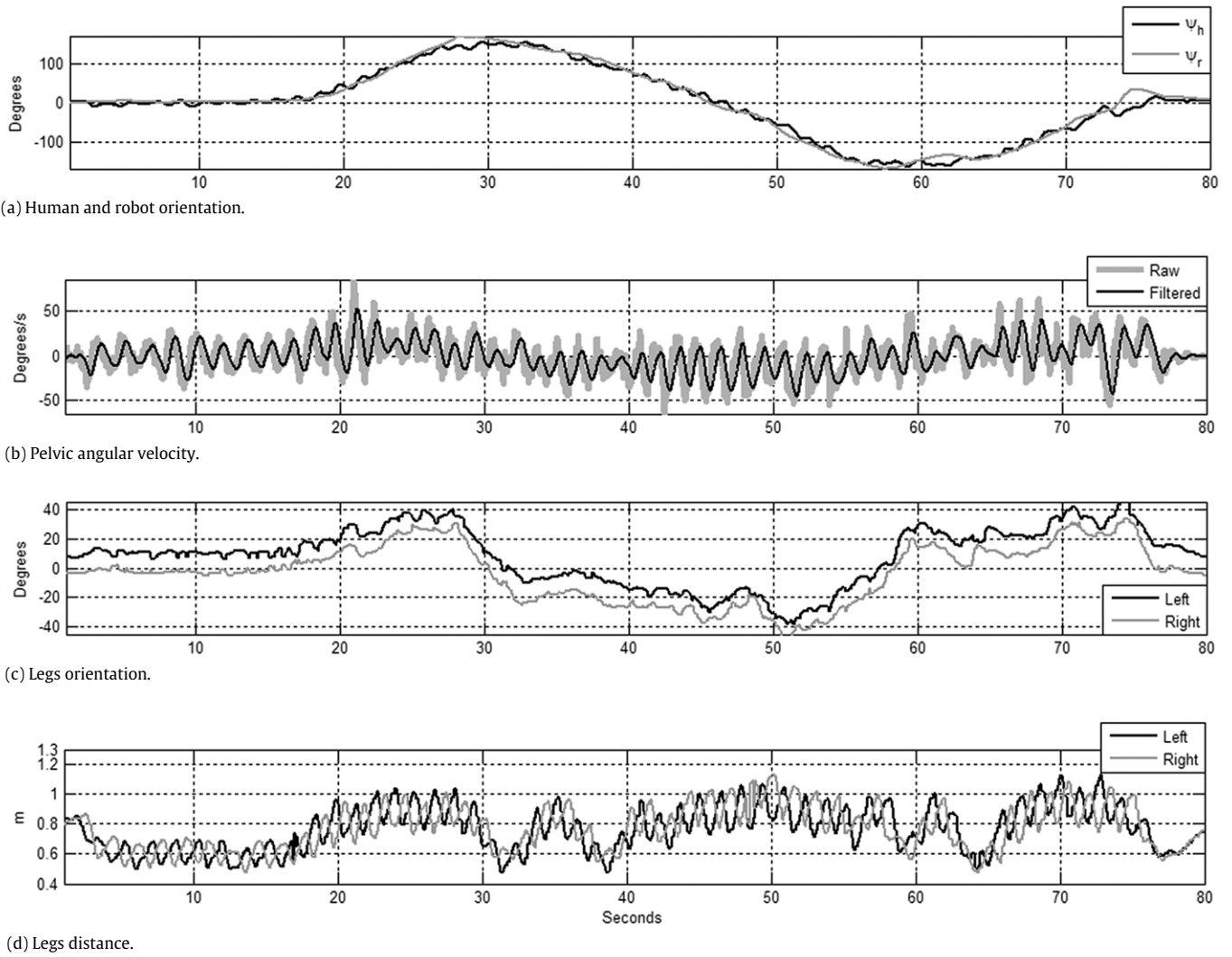
of ω_h, but also there is an expected delay between $\omega_r(C)$ and $\omega_r(R)$, which is smaller than the delay between $v_r(C)$ and $v_r(R)$.

Finally, the trajectory performed during this test is shown in Fig. 19e. The black dashed line is the human path measured from the LRF, and the gray line represents the mobile robot path measured by the robot odometry. The triangles marks represent the starting and final points of every path.

5. Conclusions and future work

This paper presented a new human–robot interaction strategy based on the human gait by data fusion from a wearable IMU and an onboard LRF. Also, a new mobile-robot human controller for tracking in front of the human with an experimental validation of the controller performance was presented.

In the experimental study, despite of the continuous oscillation during the walking, the parameters estimation was precise and

(a) Human and robot orientation.

(b) Pelvic angular velocity.

(c) Legs orientation.

(d) Legs distance.

Fig. 17. Sensors data of robot following in front experiment performing an eight-shaped curve. (a) Human and robot orientation from IMU and robot odometry respectively. (b) Pelvic angular velocity from gyroscope (raw data and filtered signal). (c) Leg orientation measured with the LRF sensor. (d) Leg distance measured with the LRF sensor.
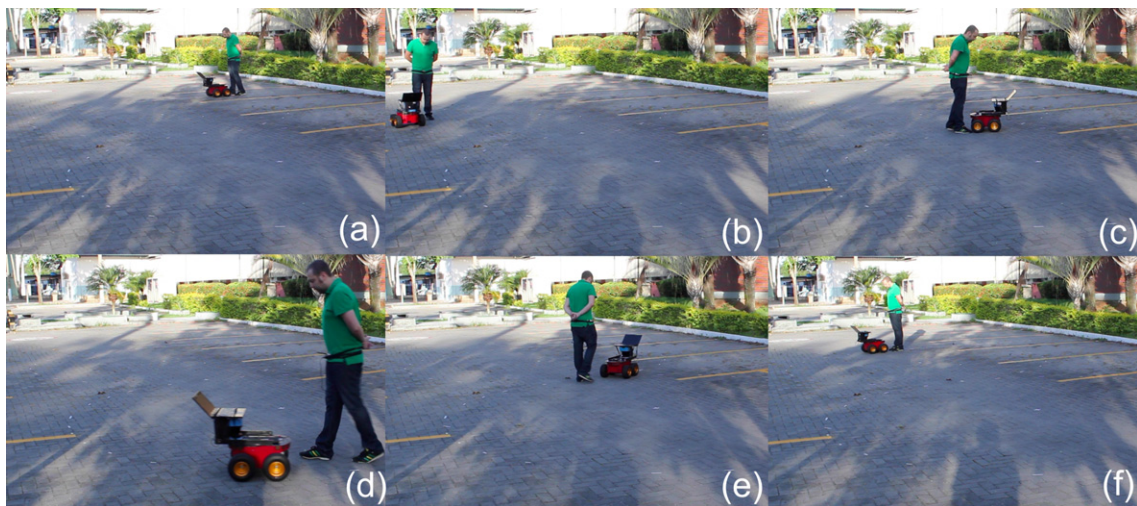
Fig. 18. Snapshots of the robot following in front experiment, performing an eight-shaped curve.

unbiased, showing also repeatability with human linear velocity changes. In the same way, the estimation errors were lower than 10% when the robot performed a curve-shaped path.

This research shows that the proposed control is effective in assisting a mobile robot to follow a human. A satisfactory result was obtained in terms of stable performance, through the
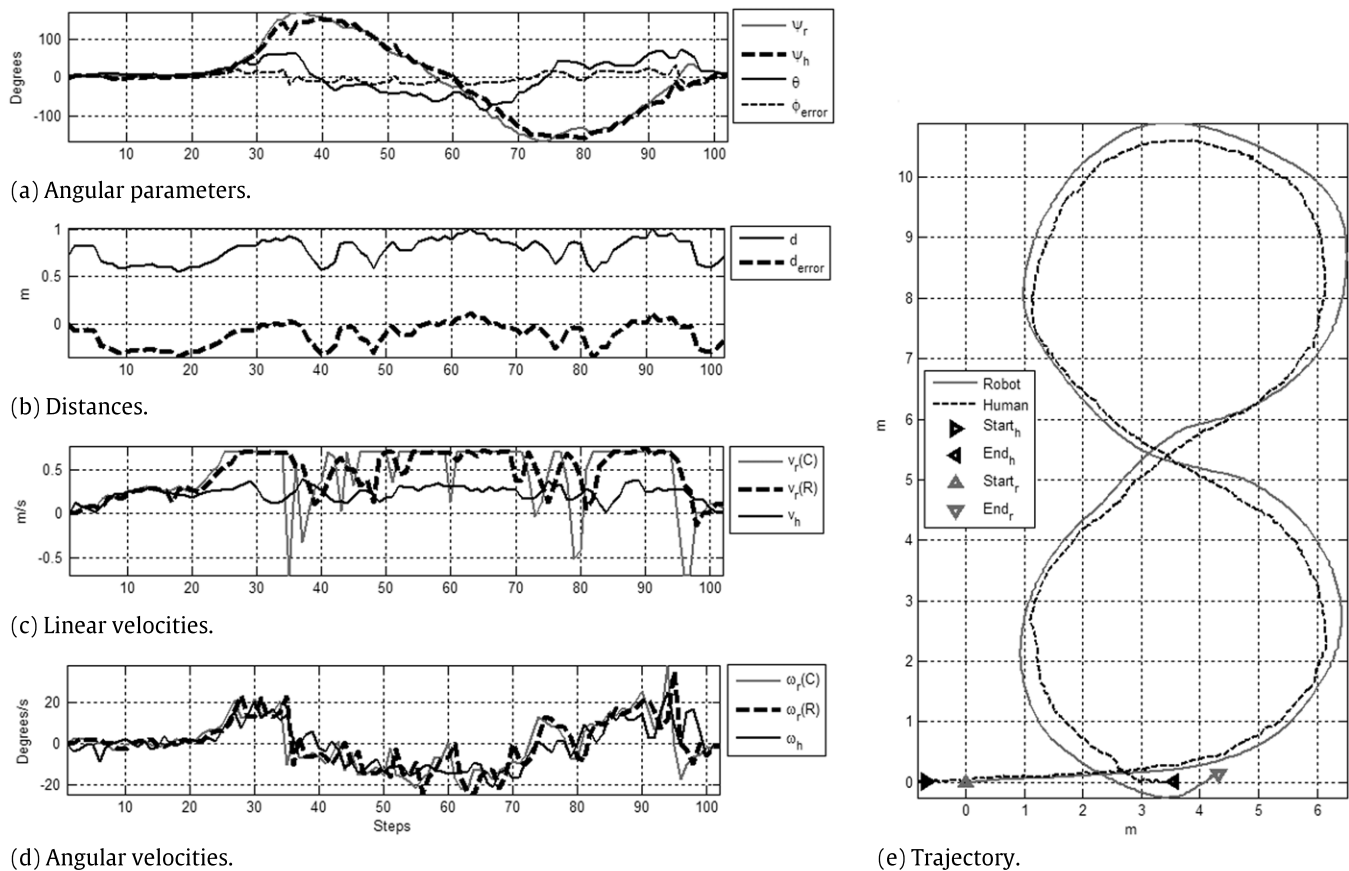
Fig. 19. Control data of robot following in front experiment performing an eight-shaped curve. (a) Angular parameters; (b) Distance parameters; (c) Linear velocities: control action $v_r(C)$ and measured $v_r(R)$ and v_h; (d) Angular velocities: control action $\omega_r(C)$, and measured $\omega_r(R)$ and ω_h; (e) Trajectory performed.

tracking algorithms here proposed. The controller was evaluated with an eight-shaped curve, showing stability of the controller even with sharp changes in the human path. The controller keeps the robot continuously following in front of the human gait in all experiments. It is also shown the good performance of the controller regarding the robot orientation when it is following the human turning during the experiments.

One of the advantages of the human-interaction here proposed is the computational efficiency due to direct measurement of the human kinematics with the IMU wearable sensor on the pelvis and the legs detection from the LRF. The detection and human tracking from the mobile robot is completed in real time and also in unstructured environments. The reliability of this approach is guaranteed with the integration of the analysis of human walking into the control parameters detection.

Acknowledgments

References

[1] IFR International Federation of Robotics, Service Robot Statistics http://www.ifr.org/service-robots/statistics/, 2013.

[2] W. Burgard, A.B. Cremers, D. Fox, D. Hähnel, G. Lakemeyer, D. Schulz, W. Steiner, S. Thrun, Experiences with an interactive museum tour-guide robot, Artif. Intell. 114 (1–2) (1999) 3–55.

[3] P. Trahanias, W. Burgard, A. Argyros, D. Hahnel, H. Baltzakis, P. Pfaff, C. Stachniss, TOURBOT and WebFAIR: web-operated mobile robots for tele-presence in populated exhibitions, IEEE Robot. Autom. Mag. 12 (2) (2005) 77–89.

[4] T. Kanda, M. Shiomi, Z. Miyashita, H. Ishiguro, N. Hagita, An affective guide robot in a shopping mall, in: Proceedings of the 4th ACM/IEEE International Conference on Human-Robot Interaction (HRI), 2009, pp. 173–180.

[5] J. Hu, A. Edsinger, Y.J. Lim, N. Donaldson, M. Solano, A. Solochek, R. Marchessault, An advanced medical robotic system augmenting healthcare capabilities—robotic nursing assistant, in: Proceedings of the 2011 IEEE International Conference on of the Robotics and Automation (ICRA), 2011, pp. 6264–6269.

[6] Z. Mohamed, G. Capi, Development of a new mobile humanoid robot for assisting elderly people, in: Proceedings of the 2012 International Symposium on Robotics and Intelligent Sensors 2012, pp. 345–351.

[7] P. Bonato, Wearable sensors and systems, IEEE Eng. Med. Biol. Mag. 29 (3) (2010) 25–36.

[8] N. Bellotto, H. Huosheng, Multisensor-based human detection and tracking for mobile service robots, IEEE Trans. Syst. Man Cybern. 39 (1) (2009) 167–181.

[9] V. Alvarez-Santos, X.M. Pardo, R. Iglesias, A. Canedo-Rodriguez, C.V. Regueiro, Feature analysis for human recognition and discrimination: application to a person-following behaviour in a mobile robot, Robot. Auton. Syst. 60 (8) (2012) 1021–1036.

[10] Y. Motai, S. Kumar Jha, D. Kruse, Human tracking from a mobile agent: optical flow and Kalman filter arbitration original, Signal Process., Image Commun. 27 (1) (2012) 83–95.

[11] D.H. Kim, Y. Lee, J.Y. Lee, G.J. Park, C.S. Han, S.K. Agrawa, Detection, motion planning and control of human tracking mobile robots, in: Proceedings of the 8th International Conference on Ubiquitous Robots and Ambient Intelligence, 2011 pp. 113–118.

[12] J. Xavier, M. Pacheco, D. Castro, A. Ruano, U. Nunes, Fast Line, Arc/Circle and Leg Detection from Laser Scan Data in a Player Driver, in: Proceedings of the 2005 IEEE International Conference on Robotics and Automation, 2005, pp. 3930–3935.

[13] S. Yoonchang, C. Woojin, Human tracking of a mobile robot with an onboard LRF (Laser Range Finder) using human walking motion analysis, in: Proceedings of the 8th International Conference on Ubiquitous Robots and Ambient Intelligence, 2011, pp. 366–370.

[14] W. Chung, H. Kim, Y. Yoo, C.B. Moon, J. Park, The detection and following of human legs through inductive approaches for a mobile robot with a single laser range finder, IEEE Trans. Ind. Electron. 59 (8) (2012) 3156–3166.

[15] D.F. Glas, T. Miyashita, H. Ishiguro, N. Hagita, Laser tracking of human body motion using adaptive shape modeling, in: Proceedings of the 2007 IEEE/RSJ International Conference on Intelligent Robots and Systems, 2007, pp. 602–608.

[16] E.J. Jung, B.J. Yi, S. Yuta, Control algorithms for a mobile robot tracking a human in front, in: Proceedings of the 2012 IEEE/RSJ International Conference on Intelligent Robots and Systems, 2012, pp. 2411–2416.

[17] S. Grzonka, F. Dijoux, A. Karwath, W. Burgard, Mapping indoor environments based on human activity, in: Proceedings of the IEEE 2010 International Conference on Robotics and Automation, 2010, pp. 476–481.

[18] G. Li, C. Zhu, J. Du, Q. Cheng, W. Sheng, H. Chen, Robot semantic mapping through wearable sensor-based human activity recognition, in: Proceedings of the 2012 IEEE International Conference on Robotics and Automation, 2012, pp. 5228–5233.

[19] L. Wu, Z. An, Y. Xu, L. Cui, Human Tracking Based on LRF and Wearable IMU Data Fusion, in: Proceedings of the 12th International Conference on Information Processing in Sensor Networks, 2013, pp. 349–350.

[20] L. Nomdedeu, J. Sales, E. Cervera, J. Alemany, R. Sebastia, J. Penders, V. Gazi, An Experiment of Squad Navigation of Human and Robots, in: Proceedings of the 10th International Conference on Control Automation, 2008, pp. 17–20. [2119] J. Ziegler, H.

[21] Kretzschmar, C. Stachniss, G. Grisetti, W. Burgard, Accurate human motion capture in large areas by combining IMU- and laser-based people tracking, in: Proceedings of the 2011 IEEE/RSJ International Conference on the Intelligent Robots and Systems. 2011, pp. 86–91.

[22] E. Prassler, D. Bank, B. Kluge, Key technologies in robot assistants: motion coordination between a human and a mobile robot, Trans. Control Autom. Syst. Eng. 4 (2002) 56–61.

[23] A. Ohya, T. Munekata, Intelligent Escort Robot Moving together with Human-Interaction in Accompanying Behavior, in: Proceedings of the 2002 FIRA Robot Congress, 2002, pp. 31–35.

[24] D.M. Ho, J.S. Hu, J.J. Wang, Behavior control of the mobile robot for accompanying in front of a human, in: Proceedings of the 2012 IEEE/ASME International Conference on Advanced Intelligent Mechatronics, 2012, pp. 377–382.

[25] K. Morioka, J.H. Lee, H. Hashimoto, Human-following mobile robot in a distributed intelligent sensor network, IEEE Trans. Ind. Electron. 51 (1) (2004) 229–237.

[26] R.C. Luo, N.W. Chang, S.C. Lin, S.C. Wu, Human tracking and following using sensor fusion approach for mobile assistive companion robot, in: Proceedings of the 35th Annual Conference of IEEE Industrial Electronics, 2009, pp. 2235–2240.

[27] M.W. Whittle, Gait Analysis: an Introduction, fourth ed., Butterworth-Heinemann Elsevier, 2007.

[28] J. Perry, J. Burnfield, Gait Analysis: Normal and Pathological Function, Slack Incorporated, 1992.

[29] M.W. Whittle, D. Levine, Three-dimensional relationships between the movements of the pelvis and lumbar spine during normal gait, Hum. Mov. Sci. 18 (5) (1999) 681–692.

[30] A. Frizera, A. Elias, A.J. del-Ama, R. Ceres, T.F. Bastos, Characterization of spatio-temporal parameters of human gait assisted by a robotic walker, in: Proceedings of the 4th IEEE RAS & EMBS International Conference on Biomedical Robotics and Biomechatronics, 2012, pp. 1087–1091.

[31] C. De la Cruz, R. Carelli, Dynamic Modeling and Centralized Formation Control of Mobile Robots, in: Proceedings of the 32nd Annual Conference IEEE Industrial Electronics, 2006, pp. 3880–3885.

[32] F.N. Martins, W.C. Celeste, R. Carelli, M. Sarcinelli-Filho, T.F. Bastos-Filho, An adaptive dynamic controller for autonomous mobile robot trajectory tracking, Control Eng. Pract. 16 (11) (2008) 1354–1363.

[33] F.G. Rossomando, C. Soria, R. Carelli, Autonomous mobile robots navigation using RBF neural compensator, Control Eng. Pract. 19 (3) (2011) 215–222.

[34] ADEPT Mobilerobots LLC, Pioneer 3-AT (P3AT) Research Robot Platform. http://www.mobilerobots.com/researchrobots/p3at.aspx, 2013.

[35] SICK, Technical Description LMS200/LMS211/LMS220/LMS221/LMS291 Laser Measurement Systems. http://www.sick-automation.ru/images/File/pdf/LMS%20Technical%20Description.pdf, 2013.

[36] C. Cifuentes, G.G. Gentiletti, M.J. Suarez, L.E Rodríguez, Development of a Zigbee platform for bioinstrumentation, in: Proceedings of the 2010 Annual International Conference of the IEEE Engineering in Medicine and Biology Society, 2010, pp. 390–393.

[37] C. Cifuentes, A. Braidot, L. Rodriguez, M. Frisoli, A. Santiago, A. Frizera, Development of a wearable ZigBee sensor system for upper limb rehabilitation robotics, 4th IEEE RAS & EMBS International Conference on Biomedical Robotics and Biomechatronics, 2012, pp. 1989–1994.

[38] T. Pallejà, M. Teixidó, M. Tresanchez, J. Palacín, Measuring gait using a ground laser range sensor, Sensors 9 (11) (2009) 9133–9146.

[39] J. Borenstein, L. Feng, Measurement and correction of systematic odometry errors in mobile robots, IEEE Trans. Robot. Automat. 12 (6) (1996) 869–880.

Carlos A. Cifuentes G. received the Biomedical Engineering master degree from Universidad Nacional de Entre Ríos, Argentina, in 2011, and is a Ph.D. student of the Robotics and Industrial Automation Group from Universidade Federal do Espírito Santo, Brazil. He is interested in rehabilitation robotics and human–machine interaction.

Anselmo Frizera Neto received the Electrical Engineering degree from Federal University of Espirito Santo (UFES), Brazil, in 2006. In 2010, he obtained his Ph.D. in Electronics from Universidad de Alcalá, Spain. From 2006 to 2010 he worked as a researcher at the Bioengineering Group, Spanish National Research Council (CSIC). Currently, he is a Professor at the Electrical Engineering Department, UFES. His research interests are rehabilitation robotics, human–machine interaction and movement análisis.

Ricardo Carelli (M'76 - SM'98) was born in San Juan, Argentina. He graduated in Engineering from the National University of San Juan, Argentina, and obtained a Ph.D. degree in Electrical Engineering from the National University of Mexico (UNAM). He is full professor at the National University of San Juan and senior researcher of the National Council for Scientific and Technical Research (CONICET, Argentina). He is Director of the Instituto de Automática, National University of San Juan (Argentina). His research interests are on Robotics, Manufacturing Systems, Adaptive Control and Artificial Intelligence Applied to Automatic Control. He is a senior member of IEEE and a member of AADECA-IFAC.

Teodiano Freire Bastos-Filho graduated in Electrical Engineering at Universidade Federal do Espirito Santo (Vitoria, Brazil), in 1987. He received his Specialization in Automation in 1989 at Instituto de Automatica Industrial (Madrid, Spain) and his Ph.D. in 1994 in Physical Science (Electricity and Electronics) at Universidad Complutense de Madrid (Spain). He is currently an Associate Professor in Universidade Federal do Espirito Santo (Vitoria, Brazil), teaching and doing research at the Postgraduate Program of Electrical Engineering, Postgraduate Program of Biotechnology and RENORBIO Ph.D. Program. His current research interests are signal processing, rehabilitation robotics and assistive technology for people with disabilities.